

# We are IntechOpen, the world's leading publisher of Open Access books Built by scientists, for scientists

6,900

Open access books available

186,000

International authors and editors

200M

Downloads

Our authors are among the

154

Countries delivered to

TOP 1%

most cited scientists

12.2%

Contributors from top 500 universities



WEB OF SCIENCE™

Selection of our books indexed in the Book Citation Index  
in Web of Science™ Core Collection (BKCI)

Interested in publishing with us?  
Contact [book.department@intechopen.com](mailto:book.department@intechopen.com)

Numbers displayed above are based on latest data collected.  
For more information visit [www.intechopen.com](http://www.intechopen.com)



# Measurement of the Polarization State of a Weak Signal Field by Homodyne Detection

Sun-Hyun Youn

*Department of Physics, Chonnam National University, Gwangju  
Korea*

## 1. Introduction

Information carried by an optical beam of light can usually be conveyed in the form of a temporal modulation of the intensity, phase, frequency or the polarization of the constituent mode(s). In that regard, homodyne detection is one of the most popular and standard method to measure the quantum mechanical properties of light Yuen & Shapiro (1978); Yuen et al. (1979); Yuen & Shapiro (1980); Yurke (1985). The quantum theory of homodyne detection originated principally from the works of Yuen and Shapiro et al. Yuen & Shapiro (1978); Yuen et al. (1979). In this method, a weak signal field is combined with a strong local oscillator field at a beam splitter, and the resulting signal is measured as a photocurrent. With the homodyne detection method, the quantum state of the signal field, such as the quadrature amplitude of the squeezed state, is easily measured Slusher et al. (1985); Wu et al. (1986); Polzik et al. (1992), and the quasiprobability distribution function can be measured by using the so-called optical homodyne tomography Smithey et al. (1993); Banaszek & W'odkiewicz (1996); Wallentowitz & Vogel (1996); Youn et al. (2001). Furthermore, optical homodyne detection is used to eavesdrop on the quantum key in quantum cryptography Hirano et al. (2000).

In quantum information science, the photon is a useful source for manipulating quantum information. To now, it has not been easy to make a consistent single-photon source, so the signal photon state is usually a weak coherent state. Therefore, it is very important to obtain the quantum state of an unknown signal field. The quantum mechanical properties of an unknown signal field, such as the amplitude squeezed state and the quadrature squeezed state, can be characterized by using the quasiprobability distribution (Wigner distribution) or the density matrix. The quasi probability distribution defines the statistical characteristics of the signal field. The well-known method to obtain quasi probability distributions (Wigner distributions) or density matrices is optical homodyne tomography Leonhardt (1997); Schiller et al. (1996).

Any kind of state reconstruction technique, however, in optical homodyne tomography requires repeated measurements of an ensemble of equally prepared signals. Therefore, this method is not adequate for finding the polarization state of a signal field that is changing pulse by pulse. Our novel scheme of polarization-modulated homodyne detection can obtain the polarization state of the signal field in a single-shot scheme. Even if the quasi probability of the signal field is not known in detail for a given single pulse, the varying polarization

state of the signal field can be obtained pulse by pulse. In this respect, our novel scheme has an advantage: It can determine the varying polarization state of the signal against the usual optical homodyne tomography.

In our earlier work Youn & Noh (2003), we proposed a polarization-controllable homodyne detection scheme for a local oscillator field whose polarization state and global phase delay were changed by using an electro-optic modulator and a piezo-electric device, respectively. In that scheme, the polarization angle and the global phase of the local oscillator field must be scanned to obtain information on the polarization state of the signal field. Therefore, the scan time is non-zero, which limits the amount of polarization information that can be obtained from the pulsed signal field. The ordinary polarization modulated homodyne detection method, which requires no scan time, can obtain polarization information on a one-time pulsed signal field Youn (2005). Polarization-modulated ordinary homodyne detection does have an advantage in that it needs only one charged coupled device, but it also has a disadvantage in that it is not free from the noise of the local oscillator field.

In section 2, we propose a polarization-modulated balanced homodyne detection method. By inserting a set of wedged wave plates in the local oscillator port, we can modulate the relative phase of the two orthogonal components as well as the overall phase retardation of the local oscillator electric field Youn & Bae (2006). Using this spatially modulated local oscillator field in the homodyne detection scheme, we can obtain the amplitudes and the relative phase of the two orthogonal components of the signal electric field. We propose a practical method to measure the polarization state of the weak signal in a single-shot scheme without any scanning time. Our proposal will be one of the essential techniques in quantum information science for reading the polarization state of an unknown signal field in a single-shot scheme.

In section 3, a polarization-modulated homodyne detection scheme using photodetectors that measure four (temporally) simultaneous photocurrent signals corresponding to four (spatially) different quadrant-shaped combinations of wave plates is proposed Youn & Jain (2009). As an extension of our previous work, we essentially do a spatial phase modulation of the two orthogonal polarization components of the local oscillator (LO) electric field by inserting a system of waveplates in the path. Information about the Jones vector associated with the signal electric field can then be obtained, and this characterization can be performed in real-time, i.e., on a single-shot basis. In particular, we also articulate an analysis to discriminate between some typical polarization states, which has implications for the security offered by standard quantum cryptographic systems.

In our current work on polarization-modulated balanced homodyne detection, we are able to determine the polarization state of the signal field on a single-shot basis. This method could be described as a hybrid of ordinary homodyne detection and quantum polarization tomography, such as the one in Ref. James et al. (2001), employing an ensemble measurement of Stokes parameters for characterizing single qubits. However, while our scheme doesn't disseminate information about the quasi-probability distribution of the signal field for a given single pulse, its usefulness comes into play in the determination of the varying polarization state of an arbitrary and unknown signal field in real-time.

In section 4, we discuss the applicability of the two methods for measuring the polarization state of a weak signal field.

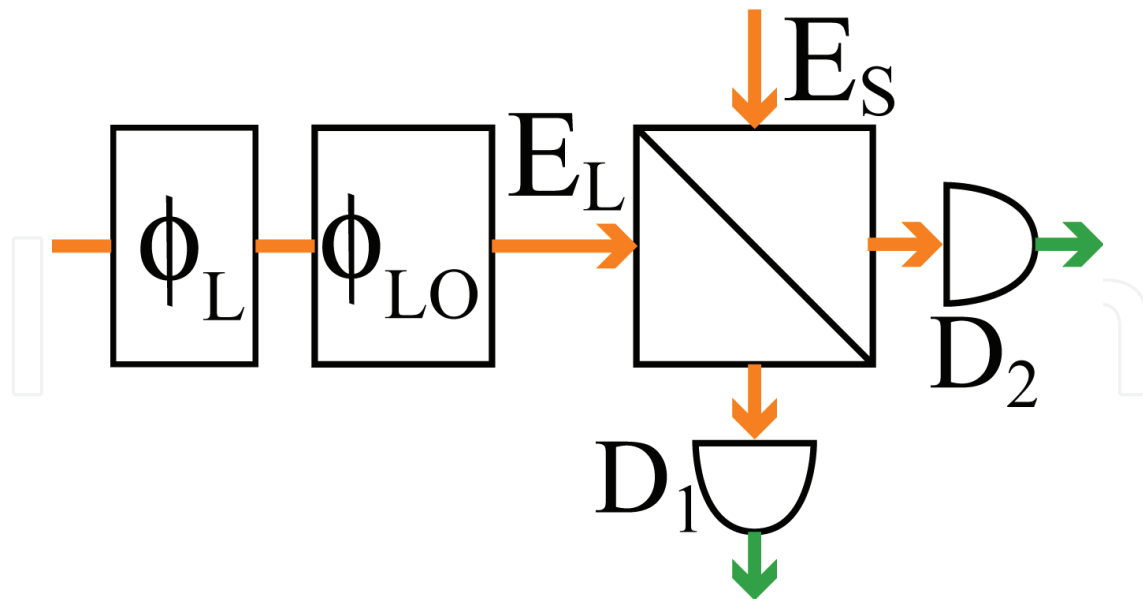


Fig. 1. Schematic diagram of polarization-controllable balanced homodyne detection.  $\phi_L$  represents the polarization state of the local oscillator.  $\phi_{LO}$  is the phase difference between the signal field and the local oscillator field ( BS: Beam splitter, D: detector, E: Electric field).

## 2. Novel scheme of polarization-modulated balanced homodyne detection for measuring the polarization state of a weak field

### 2.1 Polarization-modulated Homodyne detection

In general, the polarizations of the signal field and the local oscillator are assumed to be linear and equal to each other. We propose a scheme for polarization-controlled balanced homodyne detection Youn & Noh (2003). When the polarizations of the signal and the local oscillator are different from each other, even the ordinary homodyne detection scheme can obtain various information about the polarization states of the signal field by varying the polarization of the local oscillator. In this paper, we propose an experimental scheme that can determine the polarization state of the input signal field by using polarization-modulated balanced homodyne detection.

The scheme of polarization-modulated homodyne detection is shown in Fig. 1. The signal and the local oscillator fields, both with arbitrary polarizations, are combined at a beam splitter (BS). The electric field in the local oscillator is given as Yariv (1989)

$$\vec{E}_{LO}(\vec{r}, t) = \left( \frac{2\hbar\omega}{\epsilon} \right)^{1/2} \left[ \vec{E}_{LO}(\vec{r}) \cos(\omega t + \phi_{LO}) + \frac{1}{2} \Delta \vec{E}_{LO}(\vec{r}, t) \right], \quad (1)$$

where  $\epsilon$  is the dielectric constant and  $\omega$  is the frequency of the local oscillator field. In Eq. (1),  $\Delta \vec{E}_{LO}(\vec{r}, t)$  is a fluctuation term, with the time average of  $\Delta \vec{E}_{LO}(\vec{r}, t)$  vanishing. The monochromatic term can be decomposed into two frequency parts as follows:

$$\begin{aligned} \vec{E}_{LO}(\vec{r}, t) &\equiv \left( \frac{2\hbar\omega}{\epsilon} \right)^{1/2} \vec{E}_{LO}(\vec{r}) \cos(\omega t + \phi_{LO}) \\ &= \vec{E}_{LO}^{(+)}(\vec{r}, t) + \vec{E}_{LO}^{(-)}(\vec{r}, t), \end{aligned} \quad (2)$$

where  $\phi_{LO}$  is the overall phase of the local oscillator field relative to the signal field, and the positive ( $\vec{E}_{LO}^{(+)}$ ) and the negative ( $\vec{E}_{LO}^{(-)}$ ) frequency component are given by

$$\begin{aligned}\vec{E}_{LO}^{(+)}(\vec{r}, t) &= \left(\vec{E}_{LO}^{(-)}(\vec{r}, t)\right)^* \\ &= \left(\frac{\hbar\omega}{2\epsilon}\right)^{1/2} \vec{E}_{LO}(\vec{r}) e^{-i\omega t} e^{-i\phi_{LO}}.\end{aligned}\quad (3)$$

In addition, the fluctuating term can be decomposed into positive and negative frequency parts as

$$\Delta\vec{E}_{LO}(\vec{r}, t) = \Delta\vec{E}_{LO}^{(+)}(\vec{r}, t) + \Delta\vec{E}_{LO}^{(-)}(\vec{r}, t). \quad (4)$$

We also put the signal field in the signal port as

$$\vec{\mathcal{E}}_s(\vec{r}, t) = \vec{\mathcal{E}}_s^{(+)}(\vec{r}, t) + \vec{\mathcal{E}}_s^{(-)}(\vec{r}, t), \quad (5)$$

where

$$\begin{aligned}\vec{\mathcal{E}}_s^{(+)}(\vec{r}, t) &= \left(\vec{\mathcal{E}}_s^{(-)}(\vec{r}, t)\right)^* = \vec{E}_s^{(+)}(\vec{r}, t), \\ \vec{E}_s^{(+)}(\vec{r}, t) &= \left(\frac{\hbar\omega}{2\epsilon}\right)^{1/2} \vec{E}_s(\vec{r}) e^{-i\omega t}.\end{aligned}\quad (6)$$

The electric fields of the local oscillator and the signal are combined at a 50-50 BS, and the resultant electric fields at ports 1 and 2 are given by

$$\begin{aligned}\vec{E}_1(t) &= \frac{1}{\sqrt{2}} \left[ \vec{\mathcal{E}}_{LO}(\vec{r}, t) - \vec{\mathcal{E}}_s(\vec{r}, t) \right] \\ &= \vec{E}_1^{(+)}(t) + \vec{E}_1^{(-)}(t), \\ \vec{E}_2(t) &= \frac{1}{\sqrt{2}} \left[ \vec{\mathcal{E}}_{LO}(\vec{r}, t) + \vec{\mathcal{E}}_s(\vec{r}, t) \right] \\ &= \vec{E}_2^{(+)}(t) + \vec{E}_2^{(-)}(t),\end{aligned}\quad (7)$$

respectively, where  $\vec{E}_{1,2}^{(\pm)}(t)$  can be written as

$$\begin{aligned}\vec{E}_1^{(+)}(t) &= \left(\vec{E}_1^{(-)}(t)\right)^* \\ &= \frac{1}{\sqrt{2}} \left[ \vec{E}_{LO}^{(+)}(\vec{r}, t) + \left(\frac{\hbar\omega}{2\epsilon}\right)^{1/2} \Delta\vec{E}_{LO}^{(+)}(\vec{r}, t) - \vec{E}_s^{(+)}(\vec{r}, t) \right], \\ \vec{E}_2^{(+)}(t) &= \left(\vec{E}_2^{(-)}(t)\right)^* \\ &= \frac{1}{\sqrt{2}} \left[ \vec{E}_{LO}^{(+)}(\vec{r}, t) + \left(\frac{\hbar\omega}{2\epsilon}\right)^{1/2} \Delta\vec{E}_{LO}^{(+)}(\vec{r}, t) + \vec{E}_s^{(+)}(\vec{r}, t) \right].\end{aligned}\quad (8)$$

Since the incident photon flux operator is proportional to the product of electric field operators which are normally ordered and since one photoelectron is generated from an incident photon, based on the assumption of ideal photodetectors, the current measured from port 1 after integration over the detection area becomes

$$\begin{aligned}
 I_1(t) &= \frac{2e\sigma_{det}}{\hbar\omega} \sqrt{\frac{\epsilon}{\mu}} \vec{E}_1^{(-)}(t) \cdot \vec{E}_1^{(+)}(t) \\
 &= \frac{ec\sigma_{det}}{2} \left\{ \vec{E}_{LO}^*(\vec{r}) e^{i\phi_{LO} + i\omega t} + \left[ \Delta \vec{E}_{LO}^*(\vec{r}) e^{i\omega t} - \vec{E}_s^*(\vec{r}) e^{i\omega t} \right] \right\} \\
 &\quad \cdot \left\{ \vec{E}_{LO}(\vec{r}) e^{-i\phi_{LO} - i\omega t} + \left[ \Delta \vec{E}_{LO}(\vec{r}) e^{-i\omega t} - \vec{E}_s(\vec{r}) e^{-i\omega t} \right] \right\}, \quad (9)
 \end{aligned}$$

where  $e$  is the electron charge,  $c$  is the speed of light in vacuum, and  $\sigma_{det}$  is the area of the detector. The current at port 2, ( $I_2(t)$ ), is obtained similarly as above. Under the assumption that the fluctuation of the local oscillator field and the intensity of the signal field is much smaller than the mean intensity of the local oscillator field, the current difference between  $I_1$  and  $I_2$  can be given by

$$\begin{aligned}
 I_1(t) - I_2(t) &= \\
 &= -ec\sigma_{det} \left\{ \vec{E}_{LO}(\vec{r}) \cdot \vec{E}_s^{(+)}(\vec{r}, t) e^{-i\phi_{LO} - i\omega t} + \vec{E}_{LO}^*(\vec{r}) \cdot \vec{E}_s^{(-)}(\vec{r}, t) e^{+i\phi_{LO} + i\omega t} \right\}. \quad (10)
 \end{aligned}$$

If we set  $\vec{E}_{LO}(\vec{r}) = A\hat{e}_L/\sqrt{V}$ , where  $\hat{e}_L$  is the Jones polarization vector,  $V$  is the mode volume, and  $A$  is a constant related to the intensity of the local oscillator field, the current becomes

$$\begin{aligned}
 I(t) \equiv I_1(t) - I_2(t) &= \\
 &= -\frac{ecA\sigma_{det}}{\sqrt{V}} \left[ \vec{E}_s^{(-)}(\vec{r}, t) \cdot \hat{e}_L e^{-i(\phi_{LO} + \omega t)} + \vec{E}_s^{(+)}(\vec{r}, t) \cdot \hat{e}_L^* e^{+i(\phi_{LO} + \omega t)} \right]. \quad (11)
 \end{aligned}$$

In the homodyne detection scheme, the frequency of the signal field is the same as that of the local oscillator field, as in Eq. (6). Therefore, the current can be expressed by

$$I(t) = -\frac{ecA\sigma_{det}}{\sqrt{V}} \left[ E_s^*(\vec{r}) e^{-i\phi_{LO}} \hat{e}_s^* \cdot \hat{e}_L + E_s(\vec{r}) e^{+i\phi_{LO}} \hat{e}_s \cdot \hat{e}_L^* \right], \quad (12)$$

where  $\hat{e}_s$  is the Jones vector associated with the polarization of the signal field. Equation (12) is the final result for the measured current difference. In the general case, when both electric fields are arbitrarily polarized,

$$\hat{e}_s = a_1 e^{i\delta_1} \hat{i} + a_2 e^{i\delta_2} \hat{j}, \quad (13)$$

$$\hat{e}_L = \cos \theta_L \hat{i} + \sin \theta_L e^{i\phi_L} \hat{j}, \quad (14)$$

we have the current as

$$I = -\frac{2ecA\sigma_{det}}{\sqrt{V}} |E_s| \left[ a_1 \cos \theta_L \cos(\delta_1 + \phi_{LO}) + a_2 \sin \theta_L \cos(\delta_2 + \phi_{LO} - \phi_L) \right], \quad (15)$$

where the amplitudes  $a_1$  and  $a_2$  are non-negative real numbers which satisfy the normalization condition  $a_1^2 + a_2^2 = 1$ , and the phase factor  $\delta_1$  and  $\delta_2$  are real numbers.

## 2.2 Method to find the polarization state of the signal field

Information on the input polarization is obtained as follows: For a given signal field defined by  $(a_1, a_2, \delta_1 - \delta_2)$ , the intensity distribution  $I$  in Eq. (15) depends on three controllable parameters,  $\theta_L, \phi_L$ , and  $\phi_{LO}$ , that are related to the local oscillator field. If we scan over  $(\phi_L, \phi_{LO})$ , we can obtain full information on the polarization state of the signal field Youn & Noh (2003). Usually, the parameters  $\phi_L$ , and  $\phi_{LO}$  are controlled by using an electro-optic modulator or a piezo electric material. An electro-optic modulator changes the polarization state of the local oscillator field, and a piezo electric material changes the path length associated with the phase delay of the local oscillator field relative to the signal field. However, it is difficult to get a full scan for a single-pulse signal because the scan needs non-zero time. In this work, we propose a new scheme which does not require any scan time. We made a spatially modulated local oscillator field to perform the scan for the  $(\phi_L(t), \phi_{LO}(t))$  space in real spatial coordinates  $(\phi_L(x, y), \phi_{LO}(x, y))$ . To get spatially dependent photocurrents for a single shot-scheme, we only have to insert wave plates in the optical path of the local oscillator field, as shown in Fig. 2. Fig. 2 shows a device consisting of three wave plates and gives  $\phi_L$  and  $\phi_{LO}$  at once. The first two wave plates consist of two isotropic wedges whose refractive indices are  $n_L$  and  $n_R$ , respectively. The first and the second wedges are sliced by the plane  $z = x \tan \alpha$ , and the length from the first wedge and to the second surface at  $y = 0$  is  $d_1$ , as in Fig. 2.

On the other hand, the third wave plate is a uniaxial crystal, such as calcite, whose refractive indices can be  $n_o$  and  $n_e$ . The adjacent surfaces of the second and the third wedges are sliced by the plane  $z = y \tan \beta$ , and at that position, the length from the second surface at  $y = 0$  to the output surface of the third wedge is  $d_2$ , as in Fig. 2. The refractive indices of the third wedge are  $n_x = n_o$  and  $n_y = n_e$ .

A ray passing horizontally to the right,  $+z$ , through the device at some arbitrary point  $(x, y)$  will traverse a thickness of  $x \tan \alpha$  in the first wedge,  $d_1 + y \tan \beta - x \tan \alpha$  in the second one, and  $d_2 - y \tan \beta$  in the third one. The beam path delay imparted to the wave by the first wedge is  $2\pi n_L x \tan \alpha / \lambda$ , and that by the second wedge is  $2\pi n_R (d_1 + y \tan \beta - x \tan \alpha) / \lambda$ . On the other hand, the refractive index of the third wedge depends on the polarization axis, so we have to calculate the wave retardation for two polarization axes. Let  $\Gamma^o$  be the wave retardation due to the three wave plates for the  $x$ -axis linearly polarized light; then  $\Gamma^o$  becomes

$$\Gamma^o(x, y) = \frac{2\pi}{\lambda} \{ n_L x \tan \alpha + n_R (d_1 + y \tan \beta - x \tan \alpha) + n_o (d_2 - y \tan \beta) \}. \quad (16)$$

and  $\Gamma^e$ , the wave retardation caused by the three wave plates for  $y$ -axis linearly polarized light becomes

$$\Gamma^e(x, y) = \frac{2\pi}{\lambda} \{ n_L x \tan \alpha + n_R (d_1 + y \tan \beta - x \tan \alpha) + n_e (d_2 - y \tan \beta) \}. \quad (17)$$

After passing through the three wedges, the incident ray falls on  $(x, y)$  as the initial Jones vector  $\frac{1}{\sqrt{2}}(\hat{x} + \hat{y})$  changes into

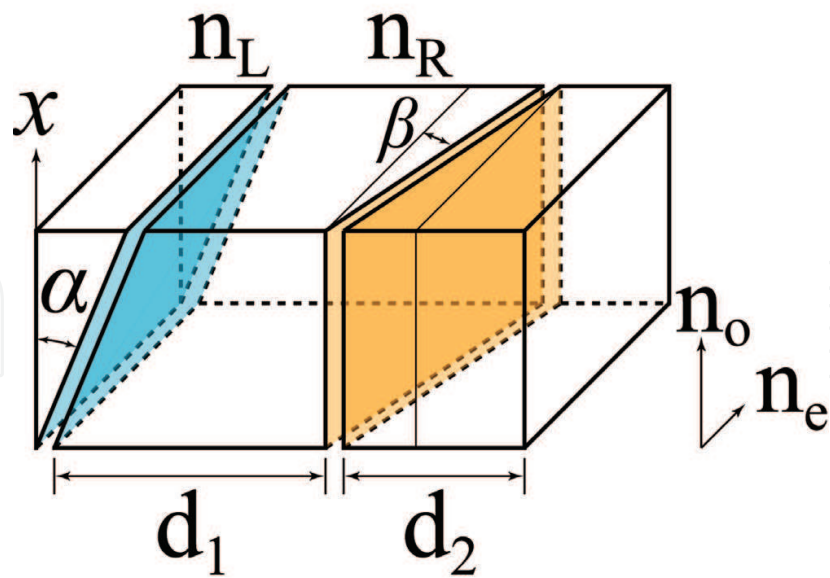


Fig. 2. Schematic diagram of two sets of wave plates with two isotropic wedges and one uniaxial wedge. The first and the second adjacent surfaces are sliced by the plane  $z = x \tan \alpha$ , and the refractive indices of the first and the second wedges are  $n_L$  and  $n_R$ , respectively. The second and the third adjacent surfaces are sliced by the plane  $z = y \tan \beta$ , and the refractive indices of the third wedge are  $n_x = n_o$  and  $n_y = n_e$ .

$$\begin{aligned} \begin{pmatrix} \hat{e}_L^x(x, y) \\ \hat{e}_L^y(x, y) \end{pmatrix} &= \begin{pmatrix} e^{i\Gamma^o(x, y)} & 0 \\ 0 & e^{i\Gamma^e(x, y)} \end{pmatrix} \begin{pmatrix} \frac{1}{\sqrt{2}} \\ \frac{1}{\sqrt{2}} \end{pmatrix} \\ &\equiv e^{i\Phi_{LO}(x, y)} \begin{pmatrix} 1 & 0 \\ 0 & e^{i\Phi_L(x, y)} \end{pmatrix} \begin{pmatrix} \frac{1}{\sqrt{2}} \\ \frac{1}{\sqrt{2}} \end{pmatrix}, \end{aligned} \tag{18}$$

where the phase factors are defined as

$$\begin{aligned} \Phi_{LO}(x, y) &= \Gamma^o(x, y) \\ &= \frac{2\pi}{\lambda} \{x(n_L - n_R) \tan \alpha + y(n_R - n_o) \tan \beta + n_R d_1 + n_o d_2\}, \end{aligned} \tag{19}$$

$$\begin{aligned} \Phi_L(y) &= \Gamma^e(x, y) - \Gamma^o(x, y) \\ &= \frac{2\pi}{\lambda} \{y(n_o - n_e) \tan \beta + (n_e - n_o)n_o\}. \end{aligned} \tag{20}$$

The overall phase delay between the signal field and the local oscillator field, and the relative phase difference between the two polarization directions ( $\hat{x}, \hat{y}$ ) are spatially modulated by one set of wave plates. In other words, by inserting one set of wave plates, we can obtain the intensity distribution of the photocurrent difference over the entire range of the two phases

$\phi_L$  and  $\phi_{LO}$ . Comparing Eq. (18) and Eq. (14), the spatially dependent photocurrent becomes

$$\begin{aligned}
 I(x, y) &= -\frac{\sqrt{2}ecA\sigma_{det}}{\sqrt{V}}|E_s|[a_1 \cos(\delta_1 + \phi_{LO}(x, y)) + a_2 \cos(\delta_2 + \phi_{LO}(x, y) - \phi_L(x, y))] \\
 &= -\frac{\sqrt{2}ecA\sigma_{det}}{\sqrt{V}}|E_s|[a_1 \cos(\delta_1 + \frac{2\pi}{\lambda}\{(n_L - n_R)x \tan \alpha + (n_R - n_o)y \tan \beta + n_R d_1 + n_o d_2\}) \\
 &\quad + a_2 \cos(\delta_2 + \frac{2\pi}{\lambda}\{(n_L - n_R)x \tan \alpha \\
 &\quad + (n_R - 2n_o + n_e)y \tan \beta + n_R d_1 - (2n_o + n_e)d_2\})], \quad (21)
 \end{aligned}$$

where we put  $\theta_L = \pi/4$  because the initial Jones vector of the local oscillator field is  $\frac{1}{\sqrt{2}}(\hat{x} + \hat{y})$ . Although we can find three parameters ( $a_1, a_2, \delta_1 - \delta_2$ ) from the modulated intensity distribution in Eq. (21), it is better to match the refractive index of the second wave plate ( $n_R$ ) with the refractive index of the third wave plate,  $n_R = n_o$ ; then, the intensity distribution in Eq. (21) becomes

$$\begin{aligned}
 I(x, y) &= -\frac{\sqrt{2}ecA\sigma_{det}}{\sqrt{V}}|E_s|[a_1 \cos(\delta_1 + \frac{2\pi}{\lambda}\{(n_L - n_o)x \tan \alpha\} + \Delta_1) \\
 &\quad + a_2 \cos(\delta_2 + \frac{2\pi}{\lambda}\{(n_L - n_o)x \tan \alpha + (n_e - n_o)y \tan \beta\} + \Delta_2)], \quad (22)
 \end{aligned}$$

where,

$$\Delta_1 = \frac{2\pi n_o(d_1 + d_2)}{\lambda}, \quad (23)$$

$$\Delta_2 = \frac{2\pi(n_o d_1 - (2n_o + n_e)d_2)}{\lambda}. \quad (24)$$

Since the intensity distribution  $I(x, y)$  depends on  $x$  and  $y$  independently, we can find the maximum value of the current  $I_{max}$  in Eq. (22) and let the values  $x_{max}$  and  $y_{max}$  be the  $x$  and  $y$  values that will yield the maximum current. When the measured values of  $x_{max}$  and  $y_{max}$  are used, the difference in the phase factor of the input polarization can be expressed as

$$\delta_2 - \delta_1 = \frac{2\pi(n_e - n_o)y_{max} \tan \beta}{\lambda} + \Delta_2 - \Delta_1 + 2m\pi, \quad (25)$$

where  $m$  is an integer. We can also obtain the magnitude of the polarization component of the input beam as

$$\begin{aligned}
 a_1 &= \frac{I_0 + I_\pi}{\sqrt{2(I_0^2 + I_\pi^2)}}, \\
 a_2 &= \frac{I_0 - I_\pi}{\sqrt{2(I_0^2 + I_\pi^2)}}, \quad (26)
 \end{aligned}$$

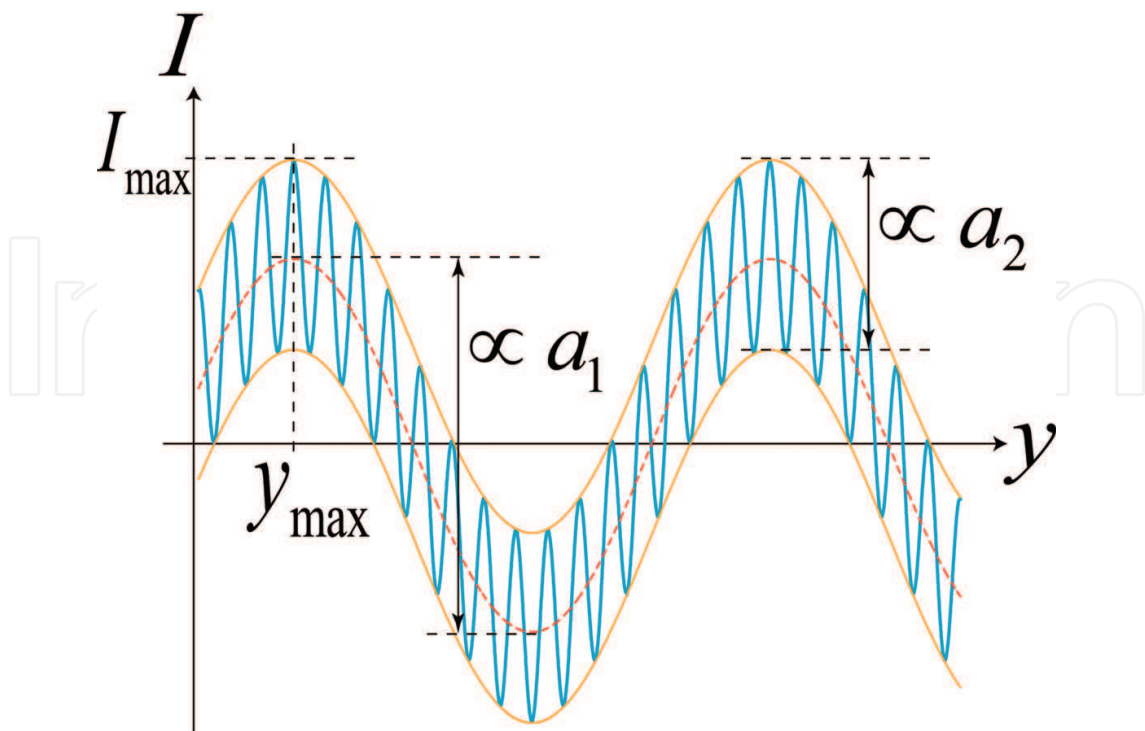


Fig. 3. Intensity modulation dependence on  $y$ . There are long- and short-term modulations whose modulation amplitudes depend on  $a_1$  and  $a_2$ , respectively.

where

$$I_{\eta} \equiv I(x_{max}, y_{max} + \frac{\lambda}{2\pi(n_e - n_o) \tan \beta} \eta). \quad (27)$$

Thus, we can obtain full information on the polarization state of the input signal field, as shown in Eq. (25) and Eq. (26). Furthermore, since our results are obtained after scanning the entire space of the phase angles  $\phi_L$  and  $\phi_{LO}$ , we do not have to fix the relative phase angle  $\phi_{LO}$  between the signal field and the local oscillator field.

Our three-wave-plate system may be simplified if we let the refractive index of the first wedge ( $n_L$ ) be the same as that of the second wedge,  $n_R = n_L$ . Then, the modulated intensity distribution becomes

$$I(y) = -\frac{\sqrt{2}ecA\sigma_{det}}{\sqrt{V}} |E_s| [a_1 \cos(\delta_1 + \frac{2\pi}{\lambda} \{(n_R - n_o)y \tan \beta\} + \Delta_1) + a_2 \cos(\delta_2 + \frac{2\pi}{\lambda} \{(n_R - 2n_o + n_e)y \tan \beta\} + \Delta_2)]. \quad (28)$$

When  $|n_R - n_o| \ll |n_R - 2n_o + n_e|$ , there are fast and slow modulation frequencies in Eq. (28), as shown in Fig. 3. From the modulated data, it becomes simple to find the values of the unknown parameters ( $a_1, a_2$ , and  $\delta_1 - \delta_2$ ) by using a fast Fourier transform or least square fitting method W. H. Press (1993).

Besides the complicated algorithm, a simple method is used to find the values of four parameters. From the intensity modulation data, we can roughly find the parameter  $a_2$ ,

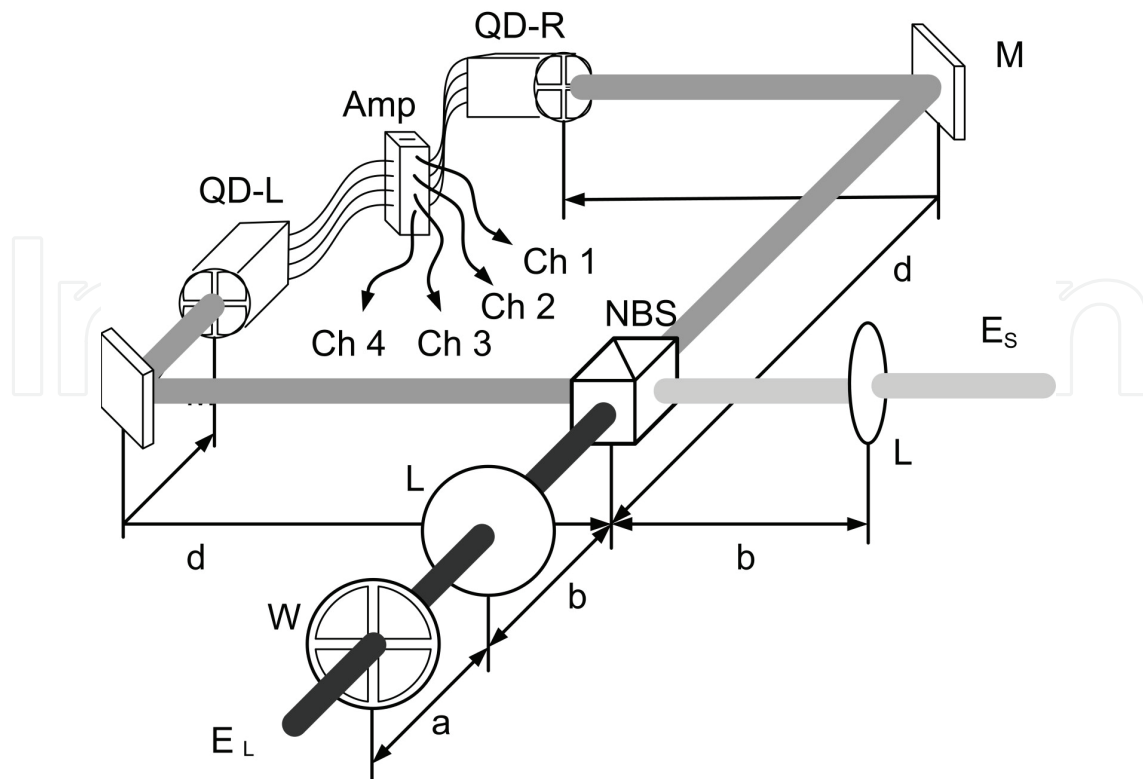


Fig. 4. Polarization-modulated homodyne detection. The organization of the waveplate quadrants for modulating the LO is explained in Fig. 5.

which is related to the short-term modulation amplitude. Furthermore, the total modulation amplitude is proportional to the sum of the two modulation amplitudes ( $a_1 + a_2$ ) as in Fig. 3. On the other hand, the phase factor  $\delta_1$  is also approximately determined at the interpolated intensity modulation peak  $I_{max}$  at  $y_{max}$  in Fig. 3. Then, the phase factor  $\delta_1$  becomes

$$\delta_1 = \frac{2\pi}{\lambda} \tan \beta(n_o - n_R)y_{max} - \Delta_1 + 2q\pi, \quad (29)$$

where  $q$  is an integer.

With the three parameters  $a_1$ ,  $a_2$ , and  $\delta_1$ , we can decide the value of the final phase factor  $\delta_2$  from the intensity modulation equation, Eq. (28). This experimental setup is very practical and easy for determining the polarization of a weak signal field.

### 3. Polarization-modulated quadrant homodyne detector for single-shot measurement of the polarization state of a weak signal field

#### 3.1 Spatial modulation of the local oscillator field

Our scheme of polarization-modulated balanced homodyne detection (BHD) is shown in Fig. 4. A signal having an unknown polarization state and a local oscillator with its polarization modulated deterministically, as per the scheme explained in the next few paragraphs, impinge on a 50:50 non-polarizing beam splitter. The spatial modulation of the LO polarization is carried out by using a four-quadrant double wave plate system.

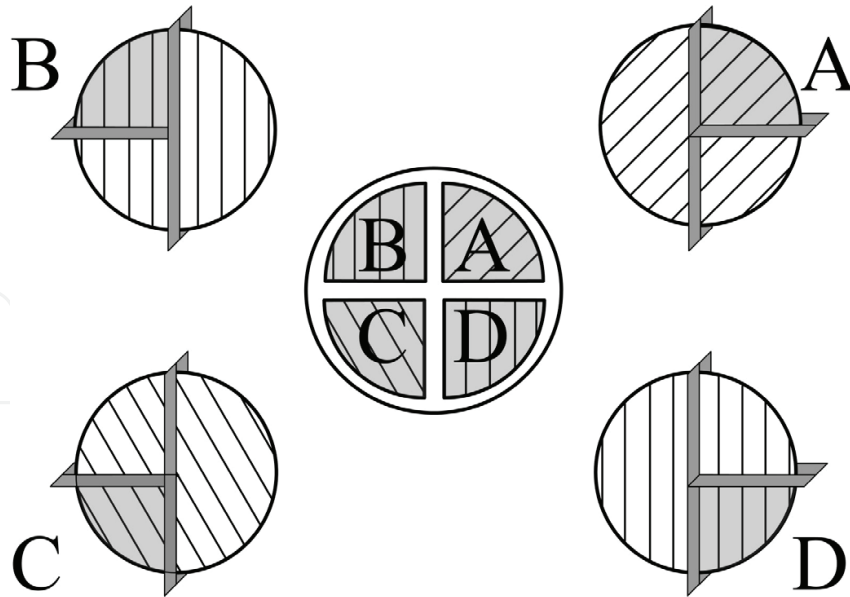


Fig. 5. Quadrant wave plate assembly: Quadrants cut from different HWPs (or QWPs) with their optical axis pre-rotated as per the requirement are glued again together to form a composite HWP (or QWP).

A de-constructed and simplified view of one of such waveplates is shown in Fig. 5. Basically, birefringent half and quarter wave plates (HWP and QWP - and at most four of each) are all cut into quadrants first. Prior to this operation, they may have to be rotated as per the polarization change that is to be induced onto the incoming field by the participating quadrant. A composite HWP (or QWP) is, thus, prepared with the four quadrants glued back together - this is similar to the idea used to make a custom-made phase modulator in the experiment by Bachor Bachor (2006). Fig. 5 shows four quadrants A-D assembled from three different (say Half) wave plates. The optical axis of the quadrants are a priori rotated by  $\pi/4$ ,  $\pi/2$ ,  $-\pi/4$  and  $\pi/2$  with respect to the horizontal. Of course, these rotation angles could really be arbitrary, but we refer to these specific values because they are employed in our computational analysis, presented in the next section. Also, it is easily observed that B and D can be cutout from one single HWP with the optical axis rotated by  $\pi/2$ , thus the need for three waveplates, in all.

With the transfer function  $\Gamma[\psi]$  of a waveplate, which induces a phase shift of  $2\psi$  between the two orthogonal polarization components, being given by

$$\Gamma[\psi] = \begin{pmatrix} e^{-i\psi} & 0 \\ 0 & e^{i\psi} \end{pmatrix}$$

and a general rotation matrix given by

$$\mathbf{R}[\theta] = \begin{pmatrix} \cos \theta & -\sin \theta \\ \sin \theta & \cos \theta \end{pmatrix}$$

the output polarization state of the LO field (with input being denoted by  $\hat{e}_L$ ), after having passed through a combination of a HWP and a QWP rotated at angles  $\alpha$  and  $\beta$ , respectively, is

given by

$$\hat{\mathbf{e}}_L^{\text{out}} = \mathbf{R}[-\alpha]\Gamma[\pi/2]\mathbf{R}[\alpha]\mathbf{R}[-\beta]\Gamma[\pi/4]\mathbf{R}[\beta]\hat{\mathbf{e}}_L. \quad (30)$$

### 3.2 Homodyne detection & polarization state measurement

As can be seen from Fig. 4, the lenses positioned in the Signal and the LO arm have a focal length  $f$  such that

$$\frac{1}{a} + \frac{1}{(b+d)} = \frac{1}{f}. \quad (31)$$

Careful alignment of these lenses serves to put one image plane each at the quadrant-based detectors QD-L and QD-R, as shown in the Fig. 4. The interference between the four spatial polarization-modulated modes of LO and the signal field (assumed to be uniform spatially) at the beam splitter is thus captured just like in an ordinary homodyne detection experiment, and taking into the account the inversion ( $A \leftrightarrow C$  and  $B \leftrightarrow D$ ), the corresponding difference photocurrent signals are amplified and obtained in channels 1-4. With the usual assumptions for a balanced homodyne detection analysis, i.e., the intensity of the signal field being much smaller than the mean intensity of the LO field, and the photodetector pair being ideal (i.e.  $\eta_L = \eta_R = 1$ ), a generic expression for the difference photocurrent  $I(t) \propto I_L(t) - I_R(t)$  is Youn & Bae (2006)

$$I(t) = -\frac{ecK\sigma_{det}}{\sqrt{V}} \left[ E_S(\vec{r})e^{i\phi_{LO}}\hat{\mathbf{e}}_L^* \cdot \hat{\mathbf{e}}_S + E_S^*(\vec{r})e^{-i\phi_{LO}}\hat{\mathbf{e}}_L \cdot \hat{\mathbf{e}}_S^* \right], \quad (32)$$

where

$e$  is the electronic charge,

$c$  is the speed of light in vacuum,

$K$  is a constant dependent on the local oscillator's field intensity,

$\sigma_{det}$  is the area of the detector,

$V$  is the mode volume,

$E_S(\vec{r})$  is the complex amplitude of the signal electric field,

$\hat{\mathbf{e}}_S$  and  $\hat{\mathbf{e}}_L$  are the Jones vectors associated with the polarization of the Signal and the LO field, respectively, and  $\phi_{LO}$  is overall phase of the LO field (relative to signal).

Again, in the general case, both electric fields are arbitrarily polarized, i.e.,

$$\hat{\mathbf{e}}_S = a_1 e^{i\delta_1} \hat{x} + a_2 e^{i\delta_2} \hat{y}, \quad (33)$$

$$\hat{\mathbf{e}}_L = b_1 e^{i\phi_{Lx}} \hat{x} + b_2 e^{i\phi_{Ly}} \hat{y}, \quad (34)$$

where  $a_i, b_i$  are real numbers and the coefficients satisfy  $a_1^2 + a_2^2 = 1, b_1^2 + b_2^2 = 1$ . In addition, if we also consider the vacuum field fluctuations that are quantum mechanically independent from the signal field, then its Jones polarization vector would be orthogonal to  $\hat{\mathbf{e}}_S$ , and would thus be of the form

$$\hat{\mathbf{e}}_V = -a_2 e^{i\delta_1} \hat{x} + a_1 e^{i\delta_2} \hat{y}. \quad (35)$$

Now, if a symmetric input polarization is employed in the local oscillator beam, i.e.,  $\hat{e}_L = 1/\sqrt{2} \hat{x} + 1/\sqrt{2} \hat{y}$ , then evaluating Eq. (30) yields the components for the output polarization,  $\hat{e}_L^{out}$ , in quadrants A, B, C and D, with pre-chosen values of  $\alpha$  (same distribution as portrayed in Fig. 5 and  $\beta$ . Table 1 lists these polarization states:

Quadrant	$\alpha$	$\beta$	$(\hat{e}_{Lx}^{out}, \hat{e}_{Ly}^{out})$
A	$\frac{\pi}{4}$	$-\frac{\pi}{4}$	$(\frac{1}{\sqrt{2}}, \frac{1}{\sqrt{2}})$
B	$\frac{\pi}{2}$	0	$(\frac{1}{\sqrt{2}}, \frac{i}{\sqrt{2}})$
C	$-\frac{\pi}{4}$	$-\frac{\pi}{4}$	$(-\frac{i}{\sqrt{2}}, -\frac{i}{\sqrt{2}})$
D	$\frac{\pi}{2}$	$-\frac{\pi}{4}$	$(-\frac{i}{\sqrt{2}}, \frac{1}{\sqrt{2}})$

Table 1. Output polarization with HWP & QWP rotated by  $\alpha$  &  $\beta$ , respectively.

Further, considering a suitable form of Eq. (32) that accounts for the effect of vacuum, as well as substituting  $\hat{e}_L^{out}$  for  $\hat{e}_L$ , in the same, yields (on simplification)

$$I(t) = -\frac{2ecK\sigma_{det}}{\sqrt{V}} \left( b_1(a_1E_S - a_2E_V) \cos(\delta_1 - \phi_{Lx} + \phi_{LO}) + b_2(a_2E_S + a_1E_V) \cos(\delta_2 - \phi_{Ly} + \phi_{LO}) \right). \quad (36)$$

Here, the  $\vec{r}$  dependence in  $E_S$  and  $E_V$  has been dropped for convenience sake, and  $\phi_{Lx}$  and  $\phi_{Ly}$  refer to the phases of the polarization components of the LO *after* the modulation, as dictated by the wave-plate assembly. Also, for non-classical fields such as the squeezed vacuum state, the difference photocurrent that constitutes terms arising from LO quantum noise and the quadrature amplitude of the signal (enhanced by the power in LO) has a statistical average of zero, i.e.,  $\langle I(t) \rangle = 0$ . For a weak coherent field however,  $\langle I(t) \rangle$  is finite and this gives us a ground to make measurements merely on  $I(t)$ , instead of the usual  $\langle I^2(t) \rangle$ . Finally, in Eq. (36), setting  $\delta_1 + \phi_{LO} \rightarrow \delta_1$  and  $\delta_2 + \phi_{LO} \rightarrow \delta_2$ , or equivalently absorbing the effect of  $\phi_{LO}$  in  $\delta_1$  and  $\delta_2$  by reducing it to zero and computing  $\phi_{Lx}$  and  $\phi_{Ly}$  from the last column of table 1, the expressions for the difference photocurrents are produced in channels 1-4 corresponding to quadrants A-D:

Quadrant	$\phi_{Lx}^{out}$	$\phi_{Ly}^{out}$	$I_{out}^v$	$I_{out}$
A	0	0	$(a_1E_S - a_2E_V) \cos \delta_1 + (a_2E_S + a_1E_V) \cos \delta_2$	$a_1 \cos \delta_1 + a_2 \cos \delta_2$
B	0	$\frac{\pi}{2}$	$-(a_1E_S - a_2E_V) \sin \delta_1 - (a_2E_S + a_1E_V) \sin \delta_2$	$-a_1 \sin \delta_1 - a_2 \sin \delta_2$
C	$-\frac{\pi}{2}$	$-\frac{\pi}{2}$	$(a_1E_S - a_2E_V) \cos \delta_1 + (a_2E_S + a_1E_V) \sin \delta_2$	$a_1 \cos \delta_1 + a_2 \sin \delta_2$
D	$-\frac{\pi}{2}$	0	$-(a_1E_S - a_2E_V) \sin \delta_1 + (a_2E_S + a_1E_V) \cos \delta_2$	$-a_1 \sin \delta_1 + a_2 \cos \delta_2$

Table 2. Photocurrent expressions for the four different quadrants. The last column corresponds to the case when vacuum fluctuations are totally neglected, i.e., when the signal field is dominant.

In general, an arbitrary (but fixed) value of the LO phase should be considered in Eq. (36). Then, replacing  $\phi_{LO}$  by  $\psi$  and an appropriate phase factor (so as to preserve the orthogonality between the *representation* of the signal polarization), the four channels' difference photocurrents for various (assumed) polarization states for the signal field can be found, as displayed in table 3.

SNo.	$\hat{e}_s$	A	B	C	D
1	(1,0)	$\cos \psi$	$-\sin \psi$	$\cos \psi$	$-\sin \psi$
2	(0,1)	$\cos(\psi - \frac{\pi}{4})$	$-\sin(\psi - \frac{\pi}{4})$	$\sin(\psi - \frac{\pi}{4})$	$\cos(\psi - \frac{\pi}{4})$
3	$\frac{1}{\sqrt{2}}(1,1)$	$\sqrt{2} \cos \psi$	$-\sqrt{2} \sin \psi$	$\sin(\psi + \frac{\pi}{4})$	$\cos(\psi + \frac{\pi}{4})$
4	$\frac{1}{\sqrt{2}}(1,-1)$	0	0	$\cos(\psi + \frac{\pi}{4})$	$-\sin(\psi + \frac{\pi}{4})$
5	$\frac{1}{\sqrt{2}}(1,i)$	$\cos(\psi + \frac{\pi}{4})$	$-\sin(\psi + \frac{\pi}{4})$	$\sqrt{2} \cos \psi$	$-\sqrt{2} \sin \psi$
6	$\frac{1}{\sqrt{2}}(1,-i)$	$\sin(\psi + \frac{\pi}{4})$	$\cos(\psi + \frac{\pi}{4})$	0	0

Table 3. Measured photocurrent values for various  $\hat{e}_s$  in the four quadrants. A phase factor of  $\frac{\pi}{4}$  is present so that the representation of  $\hat{e}_s = (1,0)$  is orthogonal to  $\hat{e}_s = (0,1)$ .

Thus, the comparative knowledge from this should make it possible to derive information about the six different signal polarization states, which also happen to be the most fundamental ( $|H\rangle$ ,  $|V\rangle$ ,  $|+\rangle$ ,  $|-\rangle$ ,  $|R\rangle$ , and  $|L\rangle$ ) in quantum information science. For example, for an experimental run, if no modulation is observed in channels A & B simultaneously, then  $\hat{e}_s = \frac{1}{\sqrt{2}}(1,-1)$ . A note of caution: since a knowledge of the absolute phase is not possible, the above expressions have been derived considering a relative phase of  $\delta = \delta_2 - \delta_1$  (refer to Eq. (33)); hence, the information is true up to a global phase. Further, using Table 3, we can now also compute error functions,  $er_i(\psi)$ , that indicate the deviation of the theoretical values from the *experimentally* measured values, i.e.

$$er_i(\psi) = \sum_{j=1}^4 (n_{ij} - o_j)^2, \quad (37)$$

where  $o_j$  is the actual value measured in the  $j^{th}$  channel, and  $n_{ij}$  is an element of the 6x4 matrix that is contained in Table 3, with rows indicated by the signal polarization and columns by the four quadrants: e.g.,  $n_{32} = -\sqrt{2} \sin \psi$ . Thus, for a given observation, Eq. (37) yields six different plots as functions of  $\psi$  and the unknown signal field polarization is indicated by the curve with the absolute minimum amongst the six.

#### 4. Conclusion and discussion

For an ensemble of equally prepared signals, the well-established optical homodyne tomography method give us the quasi probability distribution of the signal field, and the quasi probability distribution defines the statistical characteristics of the signal field, such as the amplitude squeezed state and quadrature squeezed state Leonhardt (1997). This method, however, is not adequate for obtaining information on a signal field that is changing pulse by pulse. Our polarization-modulated homodyne detection scheme is able to obtain the polarization state of a signal field in a single-shot scheme. Although the quasi probability of the signal field for a given single pulse cannot be known, we can determine the varying polarization state of the signal field pulse by pulse. Our novel scheme can determine the varying polarization state of the signal and can be used in quantum information science.

We propose a novel homodyne detection method to measure a polarization state of a weak field. At first we introduced a novel scheme of polarization modulated balanced homodyne detection method. By inserting a set of wedged wave plate in the local oscillator port, we

can modulated the relative phase of the two orthogonal components as well as the overall phase retardation of the local oscillator electric field. Using this spatially modulated local oscillator field in the homodyne detection scheme, we can obtain the amplitudes and the relative phase of the two orthogonal components of the signal electric field. It's a practical method to measure the polarization state of the weak signal in a single-shot scheme without any scanning time.

Note that, of course, other schemes may be able to measure the state of the polarization of a pulsed weak signal at once: for example, dividing the signal into many beams, measuring them with polarization-measurement setups, and finally deriving the polarization state of the input signal electric field. However, it is not practical, especially, for very weak beams because a divided beam is too weak for measurement, so the loss is not negligible. In our scheme, in some sense, we also divided the signal field spatially, but the strong local oscillator field plays a role in measuring the weak beam by a kind of amplification as in the usual homodyne detection scheme.

The second polarization-modulated homodyne detection scheme uses photodetectors that measure four simultaneous photocurrent signals corresponding to four different quadrant shaped combination of wave plates. We make a spatial phase modulation of the two orthogonal polarization components of the local oscillator electric field by inserting a system of wave plates in the path. Information about the Jones vector associated with the signal field can then be obtained, and characterization can be performed in real time, i.e., on a single shot basis.

The subtle aspect in our scheme is representing the polarization of photons, i.e., a qubit system, in a higher (four) dimensional space, thus allowing for a better discrimination between any two polarization states. To elaborate, if the quadrant-measured values are taken as components of a four-dim vector, then an orthogonality between two different signal polarization states is preserved in this new representation. Further, it includes the power of homodyne detection, which allows a measurement of a very weak or highly attenuated field, by amplifying it sufficiently. This new scheme might have application in bio-physics, where we have to measure the polarization change of the very weak beam from a single molecule.

## 5. Acknowledgements

I would like to thank Samyong Bae and Nitin Jain for their valuable work for this article.

## 6. References

- H. P. Yuen and J. H. Shapiro, *IEEE Trans. Inf. Theory* 24, 657 (1978).
- J. H. Shapiro, H. P. Yuen, and J. A. Machado-Matta, *IEEE Trans. Inf. Theory* 25, 179 (1979).
- H. P. Yuen and J. H. Shapiro, *IEEE Trans. Inf. Theory* 26, 78 (1980).
- B. Yurke, *Phys. Rev. A* 32, 311 (1985).
- R. E. Slusher, L. W. Hollberg, B. Yurke, J. C. Mertz, and J. F. Valley, *Phys. Rev. Lett.* 55, 2409 (1985).
- L-A. Wu, H. J. Kimble, J. H. Hall, and H. Wu, *Phys. Rev. Lett.* 57, 2520 (1986).
- E. S. Polzik, J. Carri, and H. J. Kimble, *Phys. Rev. Lett.* 68, 3020 (1992).
- D. T. Smithey, M. Beck, M. G. Raymer, and A. Faridani, *Phys. Rev. Lett.* 70, 1244 (1993).

- K. Banaszek and K. W'odkiewicz, *Phys. Rev. Lett.* 76, 4344 (1996).
- S. Wallentowitz and W. Vogel, *Phys. Rev. A* 53, 4528 (1996).
- S. H. Youn, Y. T. Chough and K. An, *J. Korean Phys. Soc.* 39, 255, (2001).
- T. Hirano, T. Konishi, and R. Namiki, quant-ph/0008037.
- A. Yariv, *Quantum Electronics* (Wiley, New York, 1989).
- U. Leonhardt, *Measuring the Quantum State of Light*, (Cambridge University Press, Cambridge, 1997).
- S. Schiller, G. Breitenbach, S. F. Pereira, T. Muller, and J. Mlynek, *Phys. Rev. Lett.* 77, 2933 (1996).
- D. S. Krahmer and U. Leonhardt, *Phys. Rev. A* 55, 3275 (1997).
- H. R. Noh and S.H. Youn, *J. Korean Phys. Soc.* 43, 1029 (2003).
- E. Hecht, *Optics* (Addison Wesley, New York, 2002).
- S. H. Youn, *J. Korean Phys. Soc.* 47, 803 (2005)
- W. H. Press *et al.*, *Numerical Recipes* second edition, (Cambridge University Press, Cambridge, England, 1993).
- M. Munroe, D. Boggavarapu, M. E. Anderson and M. G. Raymer, *Phys. Rev. A* 52, R924 (1995).
- C.H. Bennet and G. Brassard, *Proceedings of IEEE Intl. Conf. on Computers Systems and Signal Processing*, Bangalore India, December 175-179 (1984).
- S.H. Youn and Nitin Jain, *J. Korean Phys. Soc.* 54, 29 (2009).
- S.H. Youn and Samyong Bae, *J. Korean Phys. Soc.* 48, 397 (2006).
- Daniel F. V. James, Paul G. Kwiat, William J. Munro, and A. G. White, *Phys. Rev. A* 64, 052312 (2001)
- H-A. Bachor, *J. Mod. Opt.* 53, 5-6, 597 (2006).



## **Photodetectors**

Edited by Dr. Sanka Gateva

ISBN 978-953-51-0358-5

Hard cover, 460 pages

**Publisher** InTech

**Published online** 23, March, 2012

**Published in print edition** March, 2012

In this book some recent advances in development of photodetectors and photodetection systems for specific applications are included. In the first section of the book nine different types of photodetectors and their characteristics are presented. Next, some theoretical aspects and simulations are discussed. The last eight chapters are devoted to the development of photodetection systems for imaging, particle size analysis, transfers of time, measurement of vibrations, magnetic field, polarization of light, and particle energy. The book is addressed to students, engineers, and researchers working in the field of photonics and advanced technologies.

### **How to reference**

In order to correctly reference this scholarly work, feel free to copy and paste the following:

Sun-Hyun Youn (2012). Measurement of the Polarization State of a Weak Signal Field by Homodyne Detection, Photodetectors, Dr. Sanka Gateva (Ed.), ISBN: 978-953-51-0358-5, InTech, Available from: <http://www.intechopen.com/books/photodetectors/measurement-of-the-polarization-state-of-a-weak-signal-field-by-homodyne-detection->

**INTECH**  
open science | open minds

### **InTech Europe**

University Campus STeP Ri  
Slavka Krautzeka 83/A  
51000 Rijeka, Croatia  
Phone: +385 (51) 770 447  
Fax: +385 (51) 686 166  
[www.intechopen.com](http://www.intechopen.com)

### **InTech China**

Unit 405, Office Block, Hotel Equatorial Shanghai  
No.65, Yan An Road (West), Shanghai, 200040, China  
中国上海市延安西路65号上海国际贵都大饭店办公楼405单元  
Phone: +86-21-62489820  
Fax: +86-21-62489821

© 2012 The Author(s). Licensee IntechOpen. This is an open access article distributed under the terms of the [Creative Commons Attribution 3.0 License](#), which permits unrestricted use, distribution, and reproduction in any medium, provided the original work is properly cited.

IntechOpen

IntechOpen